2 Experimental methods

The material used for these tests was Cr–Mo steel, the chemical composition of which is shown in Table 1. Round bar (rod) specimens were heated at 860 °C as a solution treatment, followed by quenching. Tempering was performed at 600 °C. The specimens were subsequently cut into rectangular specimens with dimensions of 100 mm×100 mm×3 mm.

Fig. 1 shows the MFC processing equipment, in which an ultrasonic transducer irradiates the water jet as it emerges from the nozzle. A swirl flow nozzle [11] was used at the tip of the WJ nozzle to increase the number and size of cavitation bubbles. The discharge pressure of the pump was about 35 MPa, the nozzle diameter was 0.8 mm, and the distance between the nozzle and the specimen was assumed to be 65 mm. The considered processing times were 2, 10, 20, and 30 min.

As shown in Fig. 2, water jet cavitation isothermally expands when the sonic pressure due to ultrasonic irradiation exceeds the Break threshold, and Rayleigh shrinkage then occurs rapidly (adiabatic compression) after the cavitation expands to a certain size. The flow cavitation including the hot spot becomes MFC by the repetition of isothermal expansion and adiabatic compression. At the same time that the MFC begins to collapse, it approaches the specimen surface.

Fig. 3 shows the shape change of a photograph taken by a high-speed camera during bubble collapse into an aspheric shape [12]. The volume of the bubble decreases, and a MJ with a columnar shape that impinges the specimen surface is formed. This phenomenon is referred to as micro forging because the MJ provides high-temperature and high-pressure processing in a microscale area. Conventional WJP produces large high-pressure (several 100 μm and approximately 1000 MPa, respectively) bubbles, whereas those produced with conventional ultrasonic waves are small (several micrometers) with high temperature (several 1000 °C). In contrast, the MJ that occurs in a bubble of MFC is a deforming liquid phase body similar to a liquid jet (column) at the terminal stage of bubble collapse, and the interior of the bubble becomes high temperature (several 1000 °C) and high pressure (approximately 1000 MPa).

In the present work, the microstructure observations were conducted using optical microscopy (OM). In preparation for observations, specimens were corroded in a 5 vol% Nital etchant solution. Prior to all post–processing characterizations, specimens were cut into 1×1 cm test samples. For the measurement of the surface potential, Kelvin probe force microscopy (KFM) was performed using a multi–compatible miniature probe microscope (AFM5200S, Hitachi High–Tech Sciences, Co., Ltd.). The measurements were carried out in the atmosphere. Residual stress was measured using an X–ray stress analyzer (MSF–3M, Rigaku Corporation) with the peak top method after measurement of the (211)

Table 1. Chemical composition of the Cr-Mo steel.

(mass%)

C	Si	Mn	P	Ni	Cr	Mo	Cu	Fe
0.37	0.32	0.81	0.014	0.012	0.95	0.15	0.14	Bal.

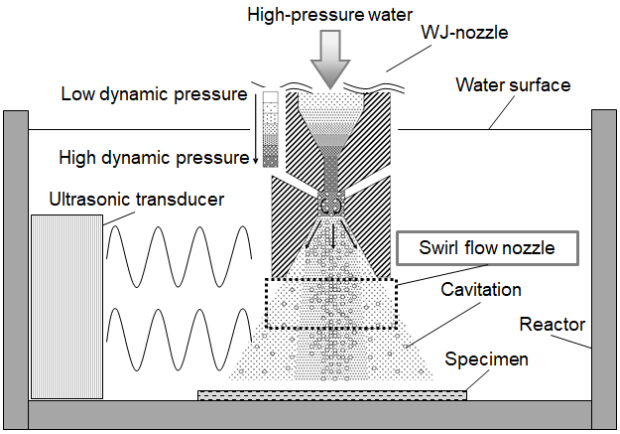

Fig. 1. Equipment for surface machining by water jet peening under ultrasonication.

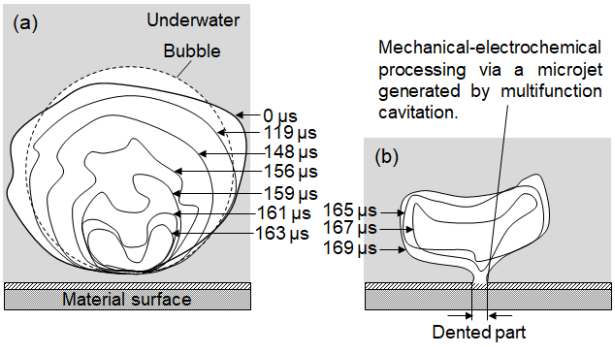

Fig. 3. A state of non-spherical collapse of bubbles. (a) 0-163 μs, (b) 165 μs~.

Fig. 2. Mechanism for MFC.

strain between lattice planes with the Cr Kα line generated at 30 kV–10 mA. The dissolved oxygen (DO) values of water in which cavitation had occurred in an SUS310S reactor for 30 min were obtained using a portable analyzer (OM – 71, Horiba, Ltd.).

3 Results discussion

To evaluate the effectiveness of the MFC processing, the residual stress was measured, and the results are shown in Fig. 4. To ascertain the effects of MFC processing, high tensile residual stress was imparted to the specimen surface by applying grinding before processing. Tensile residual stress (+179 MPa) was applied to the abraded material in the direction parallel to grinding, and it was confirmed that a nonzero compressive residual stress (−158 MPa) was present in the direction perpendicular to grinding. This phenomenon indicates that rust abnormally formed on the specimen surface when processing was applied for longer than 20 min.

Photographs of the specimen surface after MFC processing are shown in Fig. 5. To specify the position being peened, oil-based ink was applied to the specimen surface prior to processing.

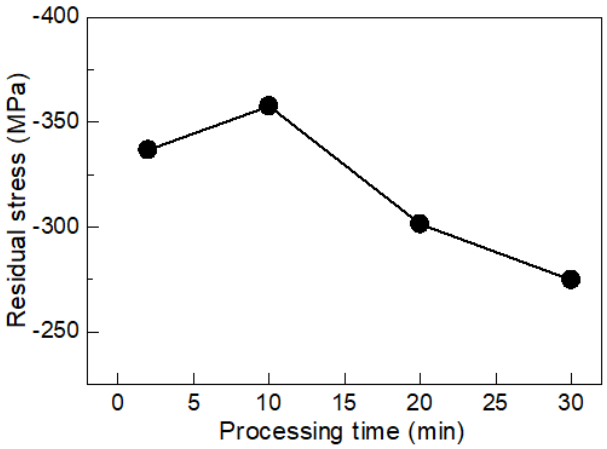

Fig. 4. Relationship between processing time and residual stress.

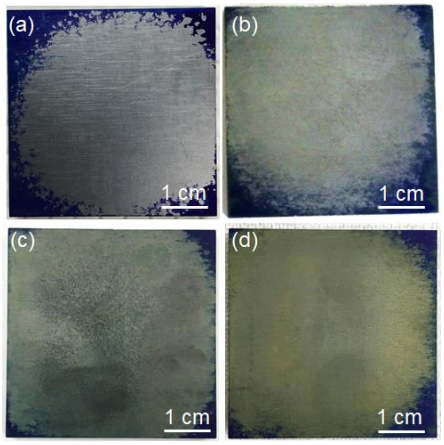

Fig. 5. Change in surface morphology as a result of MFC treatment for (a) 2 min, (b) 10 min, (c) 20 min, and (d) 30 min.

Grinding scratches were observed on the surface of specimens with a processing time of 2 min, but such grinding flaws were nearly absent for specimens processed for longer than 10 min. Furthermore, the specimen surface became bright yellow after processing for longer than 20 min, and 30 min of processing generated a large amount of the bright yellow color products on the specimen surface.

The KFM results, which give an indication of the surface condition of the specimens, are shown in Fig. 6. Because KFM involves the detection of the displacement of a cantilever due to the electrostatic attractive force on the specimen surface, it is possible to obtain the work function difference (contact potential difference) between the needle and the specimen surface. The electrostatic force received by the probe from the fixed charge distributed on the specimen surface can be detected using KFM to obtain the surface potential. The surface potential of the abraded specimen prior to MFC treatment was 234 mV. The surface potential of the specimens increased with increasing processing time until reaching a maximum value of 648 mV at 10 min and subsequently decreased with further increases to the processing time. At the longest considered processing time of 30 min, the surface potential of the treated specimen was lower than that of the abraded untreated specimen.

Fig. 7 shows optical microscopy (OM) images of the cross section of specimens after abrasion and after MFC treatment for each considered processing time.

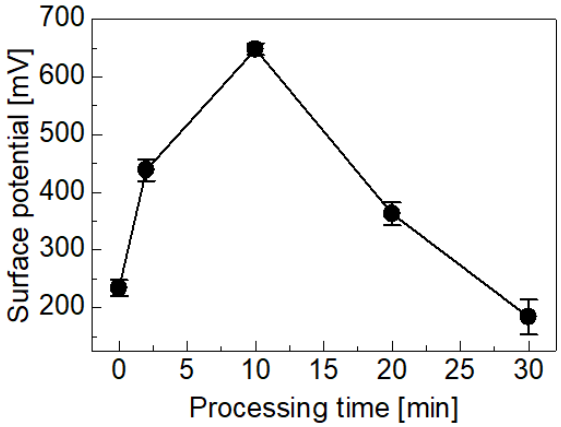

Fig. 6. Relationship between surface potential and processing time.

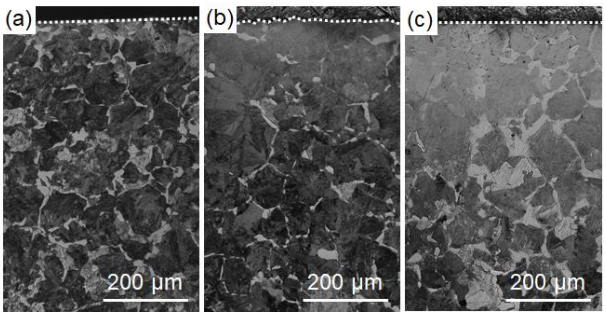

Fig. 7. Optical micrographs of the cross sections of (a) an abraded specimen and specimens treated by MFC for (b) 2 min and (c)30 min. The dashed line indicates the specimen surface.

The grain size in the depth direction from the surface after processing at each considered processing duration did not change greatly from case to case. However, in the vicinity of the surface, when the processing time was prolonged, it was observed that the color of the surface became white, with the color change progressing from the surface inward. Regarding the color of the crystal grains in the OM photograph, black grains are perlite, and white grains are ferrite. Thus, the whitening of the specimens shows that MFC processing causes pearlite existing near the processed surface to disappear. The likely cause of this is considered to be diffusion decarburization. In general decarburization, oxygen in the atmosphere and carbon in the steel combine on the steel surface during heating. This is caused by carbon scattering from the steel in the form of carbon monoxide and carbon dioxide gas. The occurrence of decarburization affects the hardness of the specimen surface. In decarburization, carbon and oxygen in steel easily bond with each other.

Fig. 8 shows the measured water temperature and DO concentrations in the water tank during MFC processing at 1200 W along with the corresponding results at 225 W obtained in a previous study [5]. When the ultrasonic output was high, the water temperature increased, and the DO concentration decreased, as shown in Fig. 8(a) and (b), respectively.

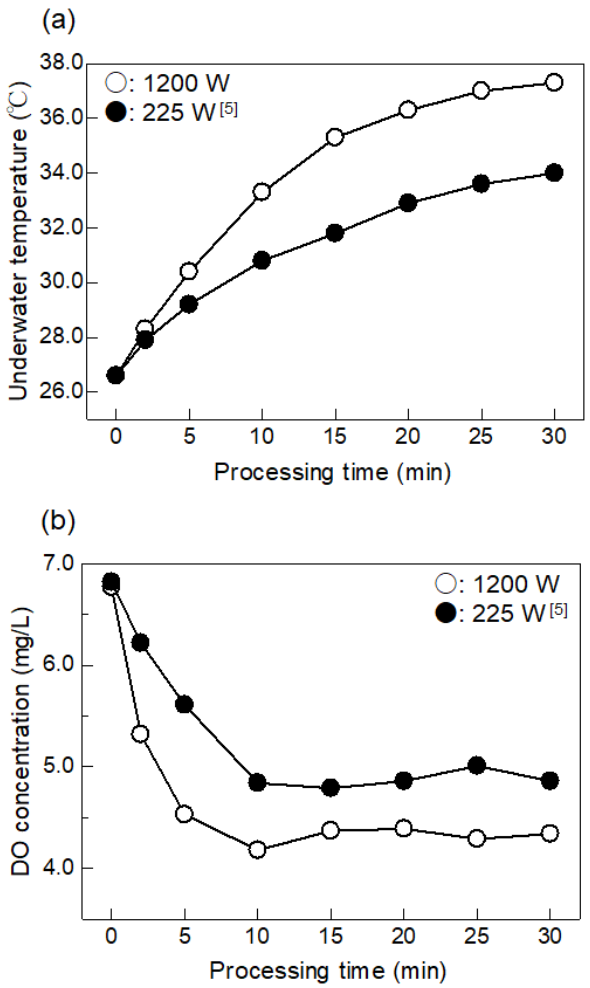

Fig. 8. Effects of processing time on (a) underwater temperature and (b) DO concentration.

The increase in the water temperature is attributable to the pressurization of the water by a high–pressure pump, which produces energy in the water flow that is partially converted into thermal energy. Regarding the reduction of the DO concentration in the water, selective oxidation occurs because of the increase in the surface temperature that occurred after 2 or 10 min of processing, causing the Cr concentration on the specimen surface to increase. It is considered that the DO concentration decreased because the Cr combined with the DO and formed an oxide film. After MFC processing for at least 20 min, the oxidized film was destroyed by cavitation bubbles. It is thus considered that the concentration of iron oxide (rust) on the surface increased as a result of the binding of DO and iron due to the Cr deficiency on the surface. The reason for the decrease in the carbon concentration on the surface after processing is considered to be as follows. As shown in Fig. 7, the color of the surface of the specimen processed for 2 min was slightly whiter than that of the unprocessed abraded specimen. It is considered that the DO and carbon on the specimen surface combined and escaped in the form of carbon monoxide or carbon dioxide gas, causing a reduction in the amount of cementite and an increase in the amount of ferrite on the surface. When diffusion decarburization occurs, the surface hardness decreases, and the fatigue strength also decreases. When applying MFC processing to various materials, it is necessary to evaluate the surface condition of the specimens after processing.

Conclusions

When applying MFC at an ultrasonic output of 1200 W, it was found that the corrosion resistance and compressive residual stress of Cr–Mo specimens were optimized by using a processing time of 10 min. However, all three of these factors decreased with increased processing time beyond this point. The reason for the deterioration of these characteristics is the occurrence of decarburization on the specimen surface. When the output power of the ultrasonic waves is high, the DO concentration decreases, the water temperature increases, and the temperature of the specimen surface increases, and these factors are thought to contribute to the occurrence of decarburization. When MFC technology is used, the amount of DO in the water, the water temperature, and the temperature of the specimen surface are affected by MFC processing, necessitating the evaluation of the specimen surface after MFC processing.

Acknowledgement

This work was supported by the Innovative Science and Technology Initiative for Security program of the Acquisition, Technology & Logistics Agency (ATLA) of Japan.

References

1. K. Hirano, K. Enomoto, E. Hayashi and K. Kurosawa, J. Soc. Mat. Sci **45** (1996) 740–745.
2. N. Saitou, K. Enomoto, K. Kurosawa, R. Morinaka, E. Hayashi, T. Ishikawa, T. Yoshimura, J. Jet. Flow Eng, **20** (2003) 4–12.
3. M. Ijiri, D. Shimonishi, D. Nakagawa and T. Yoshimura, Mater. Sc, Appl., **8** (2017) 708–715.
4. M. Ijiri, T. Yoshimura, J. Mater. Process. Tecg., **251** (2018) 160–167.
5. M. Ijiri, D. Shimonishi, D. Nakagawa, K. Tanaka and T. Yoshimura, J. Mater. Sci. Eng A., **7 (11-12)** (2017) 290–296.
6. D. Odhiambo, H. Soyama, Inter. J. Fatifue, **25** (2003) 1217–1222.
7. T. Yoshimura, K. Tanaka, N. Yoshinaga, J. Jet. Flow Eng **32** (2016) 10–17.
8. T. Yoshimura, K. Tanaka and N. Yoshinaga, Nanosci. Nanotechnol.–Asia **8** (2018) 41–54.
9. T. Yoshimura, K. Tanaka and N. Yoshinaga, BHR Group 2016 Water Jetting (2016) 223–235.
10. M. Ijiri, T. Yoshimura, 2018 IOP Conf. Ser.: Mater. Sci. Eng. **307** (2018) 012040.
11. M. Ijiri, D. Shimonishi, D. Nakagawa and T. Yoshimura, Int. J. Lightweight Mater. Manufac. **1** (2018) 12–20.
12. C. L. Kling and F. G. Hammitt, J. Basic Eng. **94** (1972) 825-833.